ADVANCED FUNCTIONAL MATERIALS
www.afm-journal.de

Dual Ion Regulated Eutectogels with High Elasticity and Adhesive Strength for Accurate Strain Sensors

Yaozhou Sun, Yin Cheng, Liangjing Shi, Jing Sun, Shuangjun Chen, and Ranran Wang**

Eutectogels have attracted increasing attention from researchers due to their broad application potential, good environmental stability, biocompatibility, and low cost. Currently reported eutectogels generally show large residue strain and hysteresis, which will cause output signal inconsistency between the loading and unloading processes and is not conducive to accurate strain monitoring. Besides, the low adhesiveness of available eutectogels brings about difficulties in the installation of the sensors and dynamic interfacial stability between the sensors and human skin. Herein, a dual ion regulation strategy is proposed to obtain eutectogels with high resilience, high adhesiveness, ultralow residue strain, wide temperature adaptability (−20–60 °C) and good environmental stability. Strain sensors based on gradient eutectogels exhibit high sensitivity, a wide linear response range, and good cycling stability. The response curve shows negligible electrical hysteresis, providing consistent output signals at the fixed strain regardless of stretch or release. Accurate micrometry with a step as minute as 50 µm is realized. Moreover, the sensors demonstrate higher signal intensity and stability in human physiological signals and motion detection due to the strong interfacial bonding.

1. Introduction

With the rapid development of the Internet of Things and artificial intelligence technology, flexible wearable sensors have shown great application prospects in the fields of health monitoring, medical diagnosis, human–machine interaction, and so on, and have attracted great attention from worldwide researchers.[1–5] Among them, flexible strain sensor not only has the advantages of being lightweight, flexible, and conformal with the human body, but also exhibits significantly higher sensitivity and sensing range compared with the traditional strain sensors, and is one of the most widely researched flexible sensors so far.

Elastic conductive composites composed of elastomer and conductive fillers have been widely investigated for flexible strain sensors. High sensitivity,[6] fast response[7] and good stability[8] have been achieved for this kind of sensor, which broadened the scope of their use. He et al. prepared a CNTs-GR/PDMS-based strain sensor with high gauge factor (GF) of 186.5, short response time of 60 ms and good stability of 10 000 cycles.[9] Nevertheless, the resistance of such sensors generally increases exponentially with strain, signifying low linearity of the sensor, which brings difficulty for quantitative analysis. Booming research work have focused on hydrogel-based flexible strain sensors in recent years due to the dominance of tunable mechanical properties, ionic conductance, self-healing, and biocompatibility.[10–12] An $A_{0.4}PC22_{1\%}$ [ChCl][EG] eutectogel prepared by Zhang et al. exhibited excellent adhesive strength (77.6 kPa), temperature adaptability (−20–80 °C), environmental stability (10 000 cycles) and sensitivity (GF = 3.17).[13] Although significant progress has been made in the development of hydrogel-based flexible sensors, there are still a couple of prominent problems to be solved. First of all, hydrogel materials should be stretchable, tough and highly resilient simultaneously to guarantee the reliability of the sensor. Unfortunately, high resilience and high toughness are seemingly contradictory for hydrogel materials. Hydrogels with high toughness usually show large residue strain, resulting in poor signal reproducibility and severe baseline drift of the sensor.[14,15] Besides, large residual strain generally exists in the stress-strain curves of these hydrogels, which is not conducive to quantitative analysis of the sensor. Second, high adhesiveness is beneficial to the conformal and intimate contact of the sensor with the skin, which is desirable for reliable and efficient signal transducing.[16] Whereas highly resilient hydrogels usually demonstrate low interfacial adhesiveness. Thirdly, the sensitivity of hydrogel-based sensors is generally lower than that of

Y. Sun, S. Chen
College of Materials Science and Engineering
Nanjing Tech University
30 Puzhu South Road, Nanjing 211816, China
E-mail: chenshuangjun@njtech.edu.cn

Y. Sun, Y. Cheng, L. Shi, J. Sun, R. Wang
State Key Laboratory of High Performance Ceramics and Superfine Microstructure
Shanghai Institute of Ceramics
Chinese Academy of Sciences
1295 Ding Xi Road, Shanghai 200050, China
E-mail: wangranran@mail.sic.ac.cn

R. Wang
School of Chemistry and Materials Science
Hangzhou Institute for Advanced Study
University of Chinese Academy of Sciences
1 Sub-lane Xiangshan, Hangzhou 310024, China

The ORCID identification number(s) for the author(s) of this article can be found under https://doi.org/10.1002/adfm.202401808

DOI: 10.1002/adfm.202401808

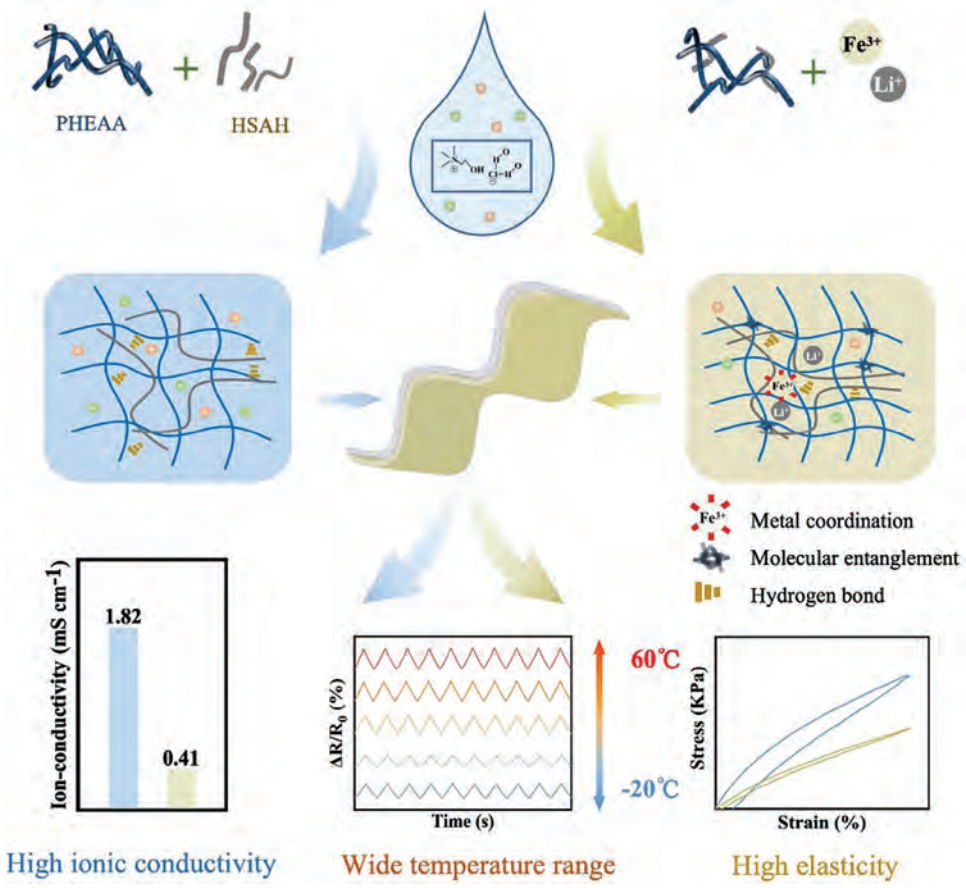

Figure 1. Design principle and properties of eutectogels with high ionic conductivity and elasticity and operable over a wide temperature range of −20–60 °C.

electronic conductive strain sensors. High ionic conductivity is essential to improve the sensitivity of hydrogels. Nevertheless, the high cross-linking degree of the polymer network that guarantees good mechanical property of hydrogels often impedes ion transport and leads to low ion conductivity. Last but not least, hydrogels gradually lose water and will freeze at sub-zero temperature, leading to changes in their mechanical and electrical properties. This will restrain the long-term use in various environments of hydrogel-based sensors. Great efforts have been made to enhance the stretchability,[17] resilience,[18] adhesion,[19] anti-drying,[20] and anti-freezing properties[21,22] of hydrogels. However, solving these problems at the same time is still a challenge.

Herein, we report a gradient eutectogel with both high stretchability (500%), low residue strain (≤6%), high adhesion, and high conductivity by adopting *(R)*−12-hydroxyethylhydrazine stearate (HSAH) and poly (N-hydroxyethyl acrylamide) (PHEAA) as the double network framework and deep eutectic solvent (DES) as the solvent (as shown in **Figure 1**). The double network framework provides good mechanical property while DES contributes to the stable and fast ion transportation. Thanks to the good conductivity, low volatility, and low freezing point of DES, the eutectogel shows high ionic conductivity, excellent environmental stability, and temperature adaptability. Through introducing the coordination effect of Fe^{3+} and the molecular entanglement effect of Li^{+}, the residue strain is further reduced while the stretchability and adhesion with substrates are greatly enhanced. The gradient eutectogel is obtained by stacking the gels with and without adding dual ions, which combines all the desired properties mentioned above. Strain sensors based on such gradient eutectogels display a wide working range, high sensitivity (GF = 2.5), high linearity, and super low electrical hysteresis of only 1.6%. The sensor can work stably in the air without encapsulation and respond accurately during the temperature range of −20–60 °C, revealing the application potential in extreme environments. Furthermore, the signal output intensity and stability are significantly enhanced compared with non-adhesive sensors in practical wearable applications, especially in the monitoring of violent motions.

2. Results and Discussion

2.1. Preparation and Structural Properties of the Eutectogel

The eutectogels were fabricated by a facile one-pot method involving mixing all ingredients homogeneously at 140 °C, and photopolymerization. During the process, HEAA monomer was polymerized by UV light initiation with Irgacure 2959 as the photo-initiator and chemical cross-linked by MBA cross-linker, forming the first network of the eutectogel. HSAH gelatinized spontaneously and fast after being dissolved in DES due to

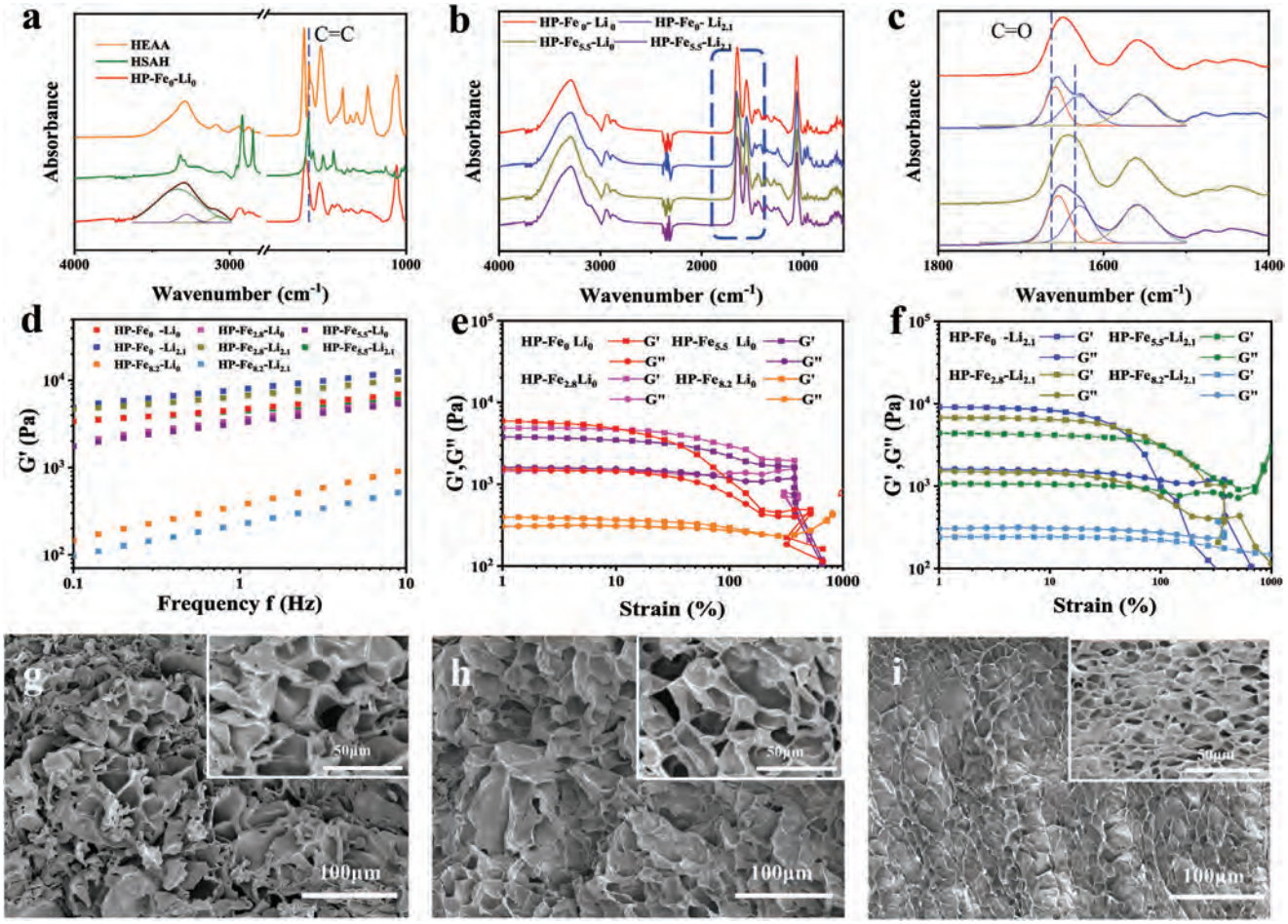

Figure 2. a–c) FT-IR spectra of HP-Fe_0-Li_0, HP-Fe_0-$Li_{2.1}$, HP-$Fe_{5.5}$-Li_0 and HP-$Fe_{5.5}$-$Li_{2.1}$ eutectogels. d) Angular frequency scanning test of HP-Fe-Li eutectogels. Angular strain scanning test results for the e) HP-Fe-Li_0 and f) HP-Fe-$Li_{2.1}$ eutectogels. g–i) SEM images of the HP-Fe_0-Li_0, HP-$Fe_{5.5}$-Li_0, and HP-$Fe_{5.5}$-$Li_{2.1}$ eutectogels.

the strong intermolecular interactions, forming the second network that interpenetrated into the PHEAA network. The cooperative intra and inter-molecular interactions of the double network guaranteed the good mechanical property of the eutectogel. Choline chloride/1,3-propanediol DES locked inside the framework provided a high ionic conductivity of 1.82 S cm^{-1}, which endowed the eutectogel with high sensitivity to strain. In order to improve the mechanical property of the eutectogel, Fe^{3+} and Li^+ were added. The FT-IR spectra (**Figure** 2a,b) analyzed the constitution, chemical and physical bonding of the eutectogel networks. The absorption peak of the HP-Fe_0-Li_0 eutectogel at 3334.5 cm^{-1} is characteristic of the —OH group, that at 3276 cm^{-1} corresponds to the stretching vibration of the —N—H group and those at 1649 and 1558 cm^{-1} are ascribed to the stretching vibration of the —C═O group and the bending vibration of the -NH group, respectively. The absence of the characteristic absorption peaks of C═C (1625 cm^{-1}) in the FT-IR spectra of the eutectogel proves that HEAA monomers have been polymerized sufficiently. The absorption peak of the —C═O group of the HP-$Fe_{5.5}$-Li_0 eutectogel red-shifts to 1642 cm^{-1}, which is attributed to the coordination of Fe^{3+} with —C═O groups.[17,23,24] The characteristic band of the carbonyl stretching vibration red-shifts from 1649 to 1629 cm^{-1} with the incorporation of Li^+, illustrating the lithium bond formation between Li^+ and carbonyl groups in HP-Fe_0-$Li_{2.1}$ eutectogel.[25,26]

SEM images (Figure 2g–i) show the microstructures of eutectogel W/O ions. The HP-Fe_0-Li_0 eutectogel exhibits non-uniform pores with large size and thick sidewalls in the crosslinked network. After adding Fe^{3+}, pores with similar sizes but thinner sidewalls are observed. Notably, the homogeneity of the crosslinked network is greatly enhanced, which may be attributed to the coordination effect between Fe^{3+} and the functional groups on polymer chains. The microstructure turns into small and dense pores in the HP-$Fe_{5.5}$-$Li_{2.1}$ eutectogel, resulting from the entanglement of polymer chains induced by the salt-out effect of Li^+.[27,28] The viscoelastic behavior of the eutectogel was measured using a rotating rheometer to investigate the effect of ions on the eutectogel. The energy storage modulus (G') and loss modulus (G'') represent the elasticity and viscosity of the material, respectively. The G' of the eutectogels was tested at different frequencies using the angular frequency sweep (FS) mode (Figure 2d), which remained essentially constant with increasing frequency. HP-$Fe_{5.5}$-$Li_{2.1}$ exhibited the smallest change in the G' among all samples with increasing frequency, demonstrating their stable elasticity through

the frequency range from 0.1 to 10 Hz. Changes in the G' and G'' of the eutectogels under different strains were measured using the angular strain sweep (AS) mode at the frequency of 1 Hz. The influence of ions on the elasticity of eutectogels was explored by comparing the G' of eutectogels with various ion concentrations. The addition of Li^+ (2.1 mg mL^{-1}) increased G' from 4720 to 8600 Pa at 1 Hz, disclosing that Li^+ significantly improved the elasticity of the eutectogel. The G' of the eutectogel at 1 Hz continuously decreases with the addition of Fe^{3+} at increasing concentrations. This trend was also observed in the eutectogels with Li^+. Changes in the G' and G'' of the eutectogels under different strains were measured using the angular strain sweep (AS) mode. With increasing strain, G' decreases and G'' increases until the intersection point is reached. When $G' > G''$, the material is in the gel state, and when $G' < G''$, the gel material is destroyed. Therefore, the intersection is an important index for judging the resistance of the gel to external damage. The analysis of the relationship between G'/G'' and strain of the eutectogels with various Fe^{3+} concentrations (Figure 2e) revealed that the resistance of the eutectogels to damage increased with the Fe^{3+} concentration owing to the formation of more dynamic bonds that enhanced the stretchability of the eutectogel. However, when the concentration of Fe^{3+} reached 8.2 mg mL^{-1}, both G' and G'' decreased greatly, which may be due to that excessive Fe^{3+} hindered the crosslink of polymer chains. The changes in the and G'' of the eutectogels containing both Li^+ and Fe^{3+} exhibited similar trend with the sample without adding Li^+ (Figure 2f). However, the G' of the eutectogels containing Li^+ was higher because of the entanglement of molecular chains. HP-Fe_0-$Li_{2.1}$ eutectogel had the highest G', however with very low strain at break (intersection strain of 90%). Comparably, although the G' of HP-$Fe_{5.5}$-$Li_{2.1}$ decreased to 4740 Pa, the resistance to damage was significantly enhanced, showing the strain at a break of 800%. Based on these features, the HP-$Fe_{5.5}$-$Li_{2.1}$ eutectogel is considered to be more suitable for the preparation of strain sensors.

2.2. Mechanical Properties of the Eutectogel

Mechanical tests have been done to analyze the influence of dual ions on the mechanical properties of eutectogels. As shown in **Figure 3a**, the tensile strength and elongation at break of the eutectogels initially increase and then decrease as the concentration of Li^+ increases from 0 to 3.2 mg mL^{-1}. The "salt-out" effect of Li^+ induces the entanglement of polymer chains that attributes to the enhanced mechanical properties. However, excessive Li^+ inhibits the polymerization of HEAA, therefore diminishing the mechanical properties of the eutectogels.[29] At the concentration of 2.1 mg mL^{-1}, the eutectogel exhibits the smallest residual strain of 2.95% during the cycling tests of 100% strain, as shown in Figure 3b,c. The addition of Fe^{3+} reduces the fracture strength and elastic modulus of the eutectogels, while increasing the elongation at break significantly (Figure 3d).[30,31] Although Fe^{3+} will increase the residue strain of the eutectogel, the coordination effect between Fe^{3+} and the functional groups on the polymer chains benefits the mechanical stability of the eutectogels, which is important for the cycle life of the sensors. Taking both resilience and mechanical stability into consideration, eutectogel with dual ions is the better choice for constructing high performance strain sensors. As shown in Figure 3g–i, at the fixed concentration of Li^+ (2.1 mg mL^{-1}), the elongation at the break of eutectogels enlarges with the increase of Fe^{3+} amount. Unlike eutectogels with only Fe^{3+}, dual ion regulated eutectogels show small residue strain until the concentration of Fe^{3+} reaches 8.2 mg mL^{-1}. The mechanical hysteresis of eutectic gels with different ionic contents is shown in Figure S3 (Supporting Information), and the trend is the same as that of the residual strain. Figure 3j shows stress-strain curves of eutectogels during 500 cycles of cyclic stretch and release tests. The breaking strength of eutectogel with only Li^+ gradually damped, which may result from the disentanglement of the polymer chains. By comparison, the breaking strength of the eutectogel with dual ions keeps steady throughout the whole cycling span, confirming the improvement in the mechanical stability of eutectogels by Fe^{3+}. Mechanical tests at different stretching speeds further demonstrate the superb resilience of the dual ion regulated eutectogels. Even if the stretching speed reaches 90 mm min^{-1}, the residue strain of HP-$Fe_{5.5}$-$Li_{2.1}$ keeps below 10% (Figure 3k).

2.3. Adhesion of the Eutectogel

In contrast to conventional elastomeric strain sensors, gel strain sensors can be made self-adherent by adjusting the gel components, thereby allowing adherence to the skin without the need for additional adhesives and consequently improving monitoring accuracy. Self-adhesion is an important advantage of gel strain sensors. The HP-$Fe_{5.5}$-$Li_{2.1}$ eutectogel exhibits excellent adhesive strength and possesses good substrate adaptability. As an interfacial binder, it can lift a weight of 500 g naturally (**Figure 4a**). The method used to test the adhesive strength is shown in Figure S4 (Supporting Information). A pressure of 20 N was applied to the eutectogels for 20 s to ensure adhesion to the substrate before the gel was pulled at a rate of 200 mm s^{-1}. The adhesive strength is defined as the maximum force applied by the eutectogels to the substrates during the stretching process. The adhesive strength of the eutectogels was tested using different substrates (Figure 4b), including carbon cloth, cu, glass, PET, PI, pigskin, PTFE, stainless steel, Ti, and Zn. The force changes between the pigskin substrate and eutectogels with different components during stretching are shown in Figure S5 (Supporting Information). The PHEAA contains hydroxyl and amide groups, and the HSAH contains hydroxyl and hydrazide groups. These groups can form hydrogen bonds with the substrate surface. Adhesion of the eutectogel to the surface of the substrate is achieved by such noncovalent interactions. The adhesive strength increases with the addition of Li^+ regardless of the substrate owing to the increase in the cohesion energy of the eutectogels. Simultaneously, Li^+ enhances the electrostatic interaction between the eutectogel and the substrate surface, which improves the adhesive strength. However, the adhesion performance with PTFE decreases upon the addition of Li^+ owing to its high polarity, thereby reducing interfacial adhesion. The addition of Fe^{3+} also enhances the adhesive strength since it induces more non-covalent bondings including coordination and hydrogen bonds on the interface (Figure 4c). Besides, the addition of Fe^{3+} decreases the modulus of the eutectogels, resulting in the formation of more dangling chains, which improves adhesion to the substrate surface.[32,33]

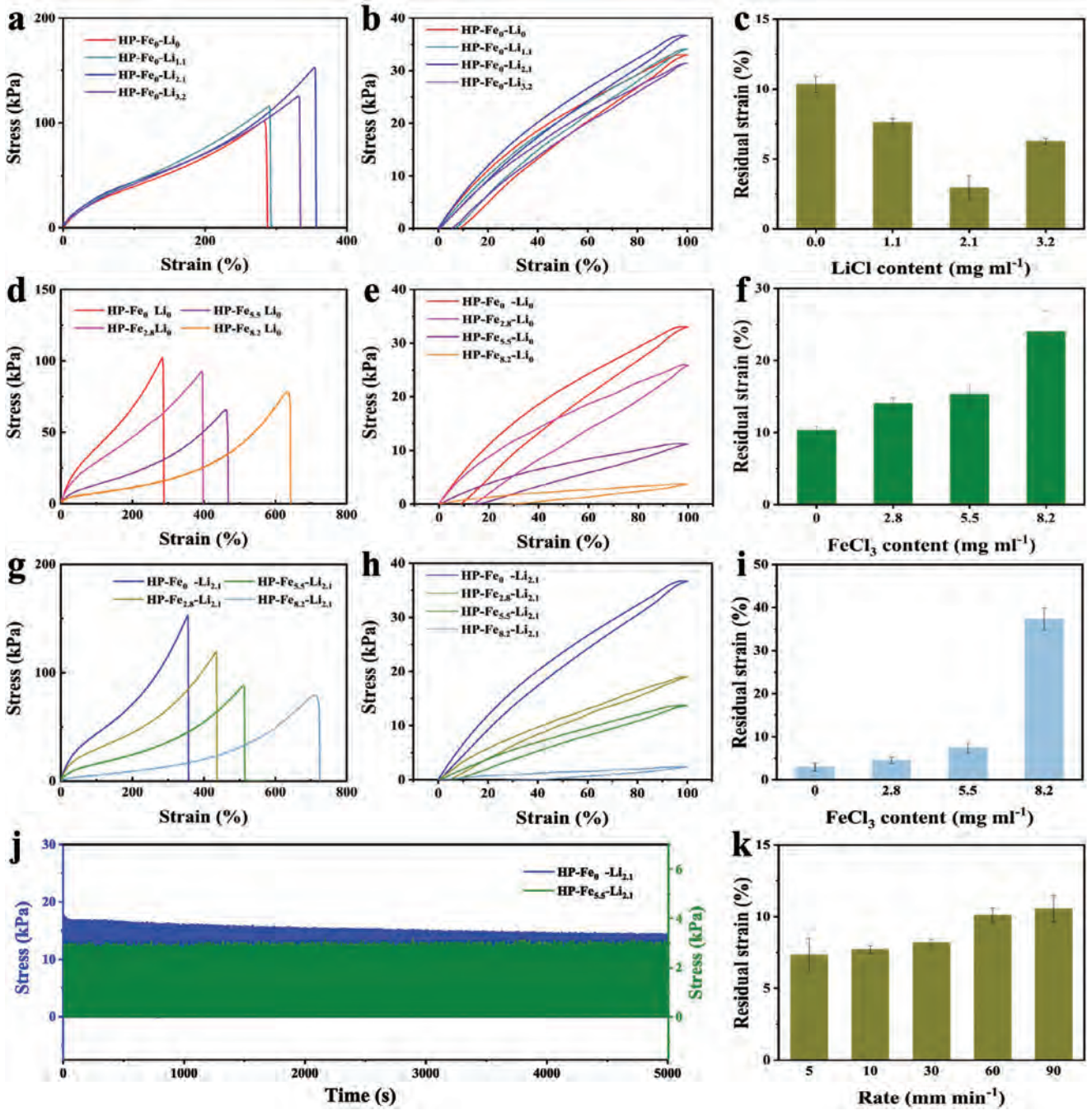

Figure 3. Tensile mechanical properties of the eutectogels. a,d,g) Tensile stress–strain curve of the HP-Fe_0-Li, HP-Fe-Li_0, and HP-Fe-$Li_{2.1}$ eutectogels. b,e,h) Cyclic loading–unloading tests of the HP-Fe_0-Li, HP-Fe-Li_0, and HP-Fe-$Li_{2.1}$ eutectogels. c,f,i) Residual strain of the HP-Fe_0-Li, HP-Fe-Li_0 and HP-Fe-$Li_{2.1}$ eutectogels at 100% strain. j) Stress of the HP-Fe_0-$Li_{2.1}$ and HP-$Fe_{5.5}$-$Li_{2.1}$ eutectogels during 500 consecutive loading–unloading cycles at a maximum strain of 100%. k) Residual strain of the HP-$Fe_{5.5}$-$Li_{2.1}$ eutectogel at 100% strain for different tensile rates.

The HP-$Fe_{5.5}$-$Li_{2.1}$ eutectogel shows excellent interface adhesive strength of over 100 kPa on various substrates, with the adhesive strength to the glass being the highest (113 kPa). In particular, the highly polar PTFE surface also exhibited an excellent adhesive strength of 107 kPa with the HP-$Fe_{5.5}$-$Li_{2.1}$ eutectogel. Pigskin, which is similar to the surface of the human body, exhibits an excellent adhesive strength of 105 kPa with the eutectogel.

Cyclic adhesion tests were conducted to evaluate the adhesion repeatability. As shown in Figure 4d, the adhesive strength of the HP-$Fe_{5.5}$-$Li_{2.1}$ eutectogel at the fifth cycle (98 kPa) was 92.02% that at the first adhesion (107 kPa), maintaining high adhesiveness after cyclic bonding and debonding. This endows the eutectogel with the potential to construct reusable wearable sensors. The adhesive strength of the HP-Fe_0-Li_0 eutectogel at the fifth

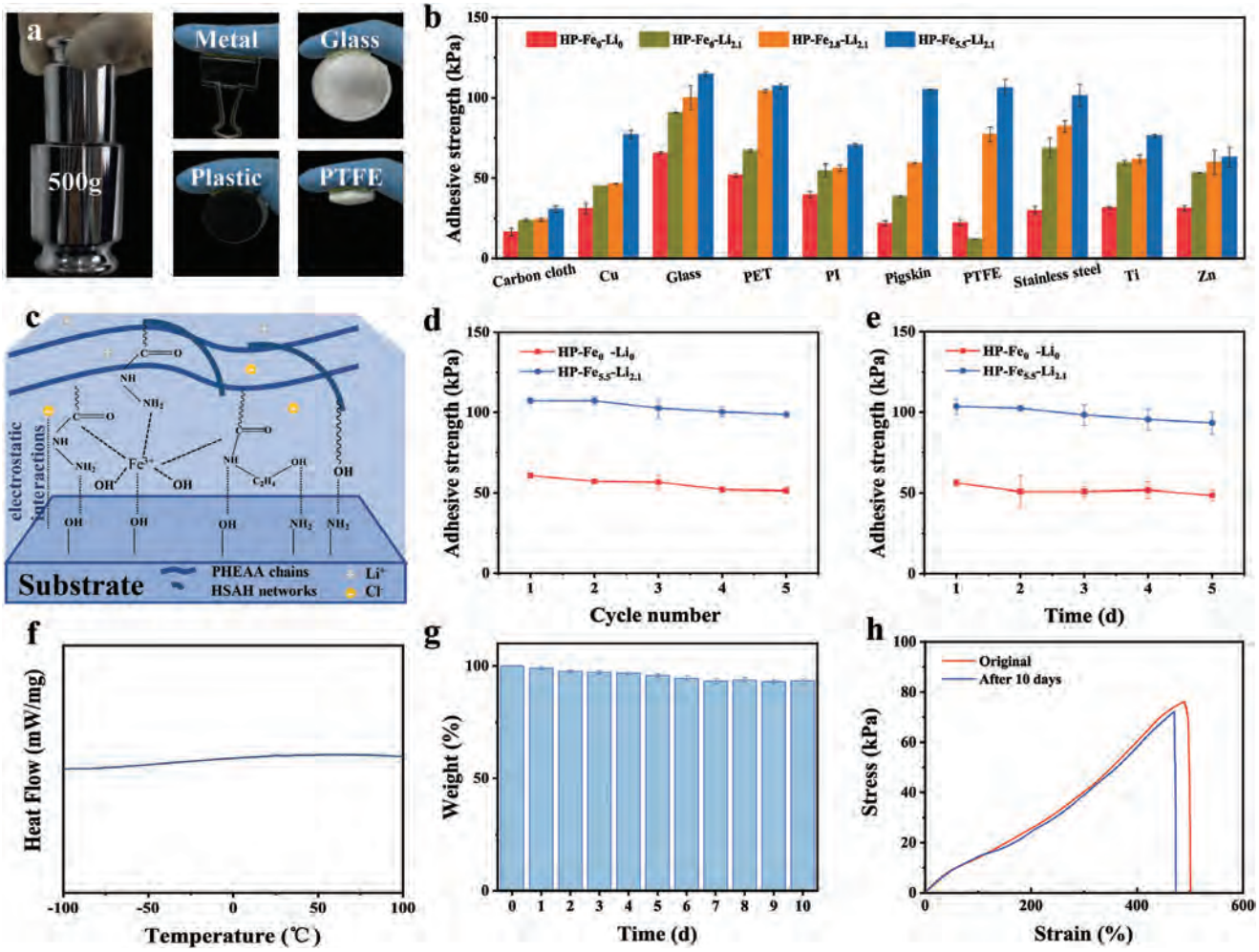

Figure 4. Adhesive properties, antifreezing, and anti-drying properties of the HP-Fe-Li eutectogels. a) Photographs of eutectogel adhesion. b) Adhesive strength of the HP-Fe_0-Li_0, HP-Fe_0-$Li_{2.1}$, HP-$Fe_{2.8}$-$Li_{2.1}$ and HP-$Fe_{5.5}$-$Li_{2.1}$ eutectogels on different substrates. c) Mechanism of adhesion of the HP-$Fe_{5.5}$-$Li_{2.1}$ eutectogel. d) Cyclic adhesive strength of the HP-Fe_0-Li_0 and HP-$Fe_{5.5}$-$Li_{2.1}$ eutectogels. e) Adhesive strength of the HP-Fe_0-Li_0 and HP-$Fe_{5.5}$-$L_{2.1}$ eutectogels stored at 25 °C for 5 d. f) DSC curve of HP-$Fe_{5.5}$-$Li_{2.1}$ eutectogel. g) Change in the mass of the HP-$Fe_{5.5}$-$Li_{2.1}$ eutectogel stored at 25 °C and 40% RH for 10 d. h) Tensile stress-strain curves of HP-$Fe_{5.5}$-$Li_{2.1}$ eutectogel before and after 10 d of storage under ambient conditions.

adhesion (52 kPa) was 86.67% that at the first adhesion (60 kPa). Both the adhesive strength and its retention ratio were lower than that of the HP-$Fe_{5.5}$-$Li_{2.1}$ eutectogel, confirming the boosting effect of the dual ion regulations.

2.4. Environmental Stability the Eutectogel

Environmental stability is of great importance for the practical application of the gels. As shown in Figure 4g, the weight of the eutectogel without encapsulation decreases slightly during the first several days and then keeps stable, confirming the superior stability of the eutectogel in the atmospheric environment at room temperature. Figure 4h demonstrates the mechanical stability of the eutectogel after being aged in the air for 10 d, which shows negligible degradation of the tensile strength and elongation at break. In addition, the adhesion capability of the eutectogels was tested by conducting the adhesion tests over 5 d (Figure 4e). The adhesive strength of the HP-$Fe_{5.5}$-$Li_{2.1}$ eutectogel on the fifth day (93 kPa) was 90.49% that on the first day (103 kPa). The adhesive strength of the HP-Fe_0-Li_0 eutectogel on the fifth day (49 kPa) was 87.5% that on the first day (56 kPa). The adhesive strength of both eutectogels remained stable over 5 d aging, demonstrating high environmental stability. Beyond that, the stability of the eutectogel over a wide temperature range was also evaluated. As shown in Figure 4f, no peak appeared on the DSC curve over the temperature range of −100-100 °C, confirming that phase transitions did not occur over this temperature range. The excellent environmental stability endows the eutectogels with the potential to be used in extreme environments.

2.5. Sensing Performance of the Eutectogel

Eutectogel strain sensors were prepared from the eutectogels with different components and fixed on a tensile table for

tensile testing (Figure S6, Supporting Information). Relative resistance changes of strain sensors based on eutectogels W/O ions were tested as the sensors were stretched to 150% strain and then returned to their initial state. As shown in **Figure 5**a, both sensors demonstrate a linear increase in the resistance with the increment of strain. The high linearity of the response curve is beneficial to the quantitative analysis of strain. The HP-Fe_0-Li_0 eutectogel-based strain sensor exhibits higher sensitivity (GF = 3.0) but larger electrical hysteresis (4.9%), while the HP-$Fe_{5.5}$-$Li_{2.1}$ eutectogel-based strain sensor shows lower sensitivity (GF = 2.2) with negligible electrical hysteresis (0.3%) (Figure S7, Supporting Information). This is mainly attributed to the densification of the hydrogel networks by adding Fe and Li ions as proved by the SEM characterization, which leads to the decrease of the ionic conductivity from 1.82 to 0.41 mS cm^{-1} as shown in Figure 5b. In order to obtain better comprehensive performance, HP-Fe_0-Li_0/HP-$Fe_{5.5}$-$Li_{2.1}$ gradient eutectogel strain sensors were constructed, among which the HP-Fe_0-Li_0 layer worked as the sensitive layer while the HP-$Fe_{5.5}$-$Li_{2.1}$ layer served as the highly elastic and self-adhesive substrates. The loading–unloading test confirms that the HP-Fe_0-Li_0/HP-$Fe_{5.5}$-$Li_{2.1}$ gradient eutectogel strain sensor exhibits both high sensitivity (GF = 2.5) and a small hysteresis loop (electrical hysteresis = 1.6%).

The HP-Fe_0-Li_0/HP-$Fe_{5.5}$-$Li_{2.1}$ gradient eutectogel strain sensor was tested at different tensile frequencies (0.1, 0.5, 1, and 2 Hz) under 0.5% strain (Figure 5c). The output signal showed no apparent change with the increase in stretching frequency, enabling their application in monitoring human motions. This feature was also demonstrated through the rheological test. The results of the three-cycle tensile test of the HP-Fe_0-Li_0/HP-$Fe_{5.5}$-$Li_{2.1}$ gradient eutectogel strain sensor at low strains (0.5%, 1%, 2%, and 5%) are shown in Figure 5d. The strain sensor has a low detection limit (0.5%) and is therefore suitable for monitoring minute strain. The results of the three-cycle tensile tests at high strains (25%, 50%, 75%, and 100%) are shown in Figure 5e. The strain sensor outputs stable electrical signals and is not damaged at high strain. These results demonstrate that the sensor can reliably monitor the full range of human activities, from weak physiological signals to intense movements. The rapid stretching and recovery test of the strain sensor (Figure 5f) reveals short stretching and recovery response times of 90 and 80 ms, respectively. The repeatability of the gradient eutectogel strain sensor was tested by cyclic stretching and releasing at 50% strain as well as cyclic bending to 90°. As shown in Figure 5g, the strain sensor outputs stable signals over 3000 cycles of stretch and recovery. In the cyclic bending tests (Figure S9, Supporting Information), the sensor outputs stable signals for 6500 cycles. These results demonstrate that the eutectogel strain sensor is suitable for long-term monitoring.

To adapt to the application under extreme conditions, a 10-cycle test was conducted under 30% strain at different temperatures (−20 °C, 0 °C, 25 °C, 40 °C, and 60 °C). As shown in Figure 5h, the HP-Fe_0-Li_0/HP-$Fe_{5.5}$-$Li_{2.1}$ gradient eutectogel strain sensor provides stable signal output over the temperature range of −20–60 °C. The high stability of the deep eutectic solvent over a wide temperature range as proved by the DSC analysis (Figure 4f) is mainly responsible for the broad environmental adaptability. Higher temperature facilitates ion transport in the eutectogel, leading to higher sensitivity of the gradient eutectogel strain sensor. Therefore, temperature correction is needed in practical applications.

2.6. Application Demonstrations of the Gradient Eutectogel Strain sensor

We demonstrated that the HP-Fe_0-Li_0/HP-$Fe_{5.5}$-$Li_{2.1}$ gradient eutectogel strain sensor had high elasticity and sensitivity. In addition, the sensor exhibited strong self-adhesion, excellent environmental stability, and other desirable characteristics. Accordingly, the eutectogel strain sensor can play a role in micrometry, human physiological signal detection and human motion monitoring. In **Figure 6**a, a micro stretch of 50 µm was applied three times to the gradient eutectogel strain sensor, and consistent resistance increment was monitored. No overshoot and plateau attenuation were observed, which is essential for quantitative analysis of strain. When unloaded, the output signal conformed to the signal in stretching, demonstrating excellent reliability of the sensor. The ultra low electrical hysteresis of the gradient eutectogel is of great importance to the consistency of the output signals during the loading and unloading stage.

Based on the high accuracy and self-adhesion of the gradient eutectogel strain sensor, it demonstrates great advantages in human physiological monitoring. The as-prepared self-adhesive and nonadhesive strain sensors were fixed to the wrist (Figure 6b), among which the nonadhesive sensors were obtained by sticking a thin layer of ecoflex film at the bottom of the adhesive sensor. The self-adhesive strain sensor outputs clear pulse waves.[10] In contrast, for the non-adhesive sensor, only a tiny signal can be observed without the characteristic peak shape of the pulse wave. This is due to the poor conformality of the non-adhesive sensors to the surface of the human skin, which is not able to capture some of minute changes. The sensor was then fixed on the lower chest of human to monitor breath. As shown in Figure 6c, both adhesive and non-adhesive sensors output regular signal change with breath. However, the output signal of the non-adhesive sensor was much weak, accompanying by many interference peaks.

In addition to detecting subtle physiological signals, self-adhesive gradient eutectogel strain sensor also demonstrates great advantages in human motion monitoring due to the strong bonded interface and the improved monitoring accuracy. The as-prepared self-adhesive and non-adhesive strain sensors were fixed to the finger and elbow (Figure 6d–g). The self-adhesive strain sensor outputs stronger signals during movement, with average signal intensities of 19.9% and 36.0% at the finger and elbow. The average output signal intensities of the nonadhesive strain sensor were significantly lower, 7.9% and 19.9% at the finger and elbow respectively. It is believed that the conformal and tightly bonded interface between the self-adhesive sensor and human skin promotes stress transfer, therefore enhancing the output signal intensity. Except for boosting the output signals, the self-adhesive property of the sensor is also beneficial to avoiding the signal disorder caused by the interfacial instability. As shown in Figure 6h,i, the self-adhesive and non-adhesive strain sensors were fixed under the wrist and were bent inward slowly and rapidly. During cyclic bending, the self-adhesive strain sensor remained intimate adhesion to the skin surface and output

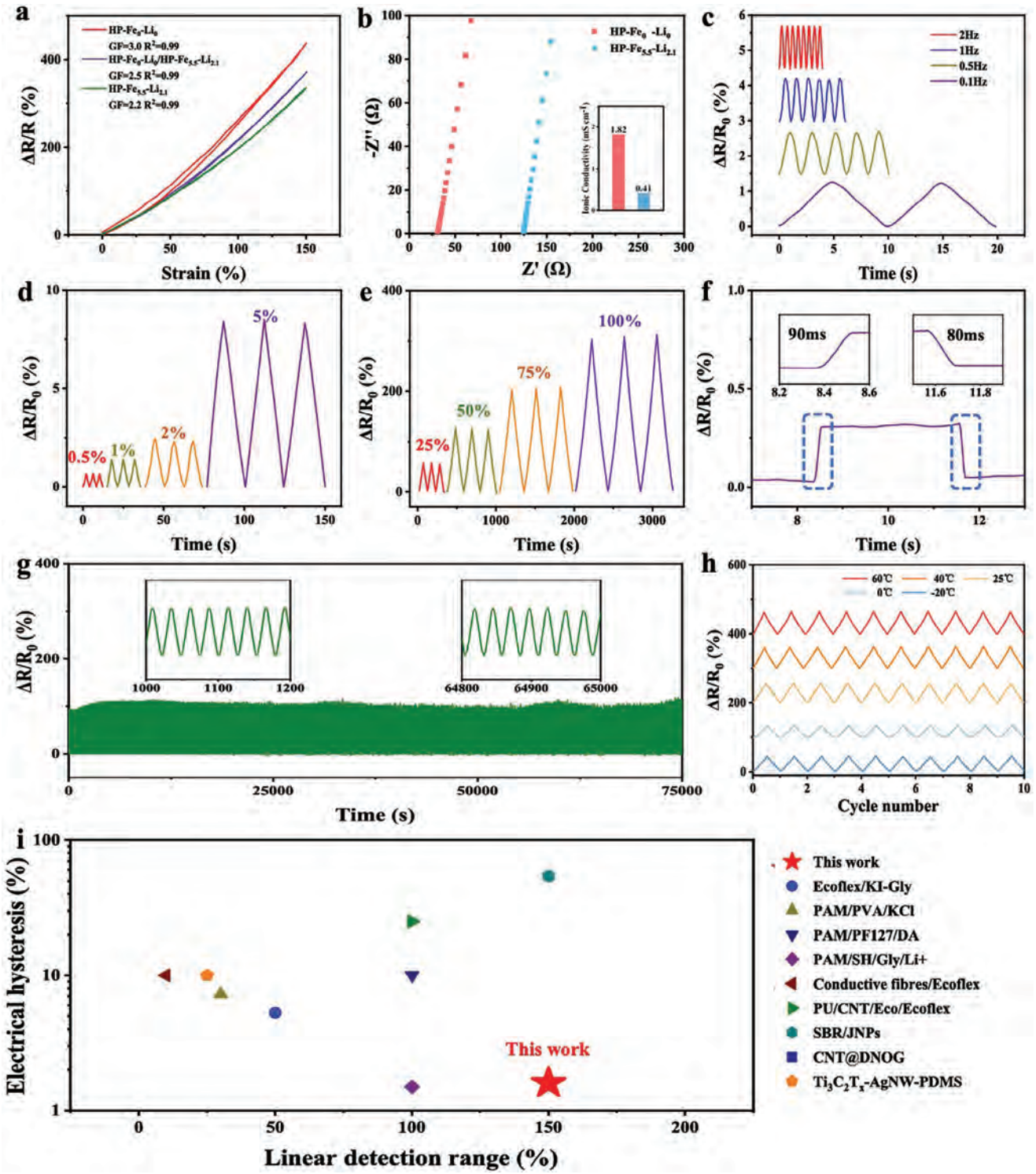

Figure 5. a) Electrical-mechanical tests for the HP-Fe_0-Li_0 and HP-$Fe_{5.5}$-$Li_{2.1}$ eutectogels and the HP-Fe_0-Li_0/HP-$Fe_{5.5}$-$Li_{2.1}$ gradient eutectogel. b) Electrochemical impedance spectra and ionic conductivities of the HP-Fe_0-Li_0 and HP-$Fe_{5.5}$-$Li_{2.1}$ eutectogels. c) Relative resistance changes of the HP-Fe_0-Li_0/HP-$Fe_{5.5}$-$Li_{2.1}$ gradient eutectogel strain sensor at different stretching frequencies. d,e) Relative resistance change of the HP-Fe_0-Li_0/HP-$Fe_{5.5}$-$Li_{2.1}$ gradient eutectogel strain sensor at different applied strains. f) Rapid tensile and recovery tests for the HP-Fe_0-Li_0/HP-$Fe_{5.5}$-$Li_{2.1}$ gradient eutectogel strain sensor. g) Relative resistance changes in the HP-Fe_0-Li_0/HP-$Fe_{5.5}$-$Li_{2.1}$ gradient eutectogel strain sensor at 50% strain over 3000 cycles. h) Relative resistance change (30% strain) of the HP-Fe_0-Li_0/HP-$Fe_{5.5}$-$Li_{2.1}$ gradient eutectogel strain sensor at different temperatures (−20 °C, 0 °C, 25 °C, 40 °C, and 60 °C). i) Sensing properties of the HP-Fe_0-Li_0/HP-$Fe_{5.5}$-$Li_{2.1}$ gradient eutectogel strain sensor compared with other strain sensors reported in the literature.[34–42]

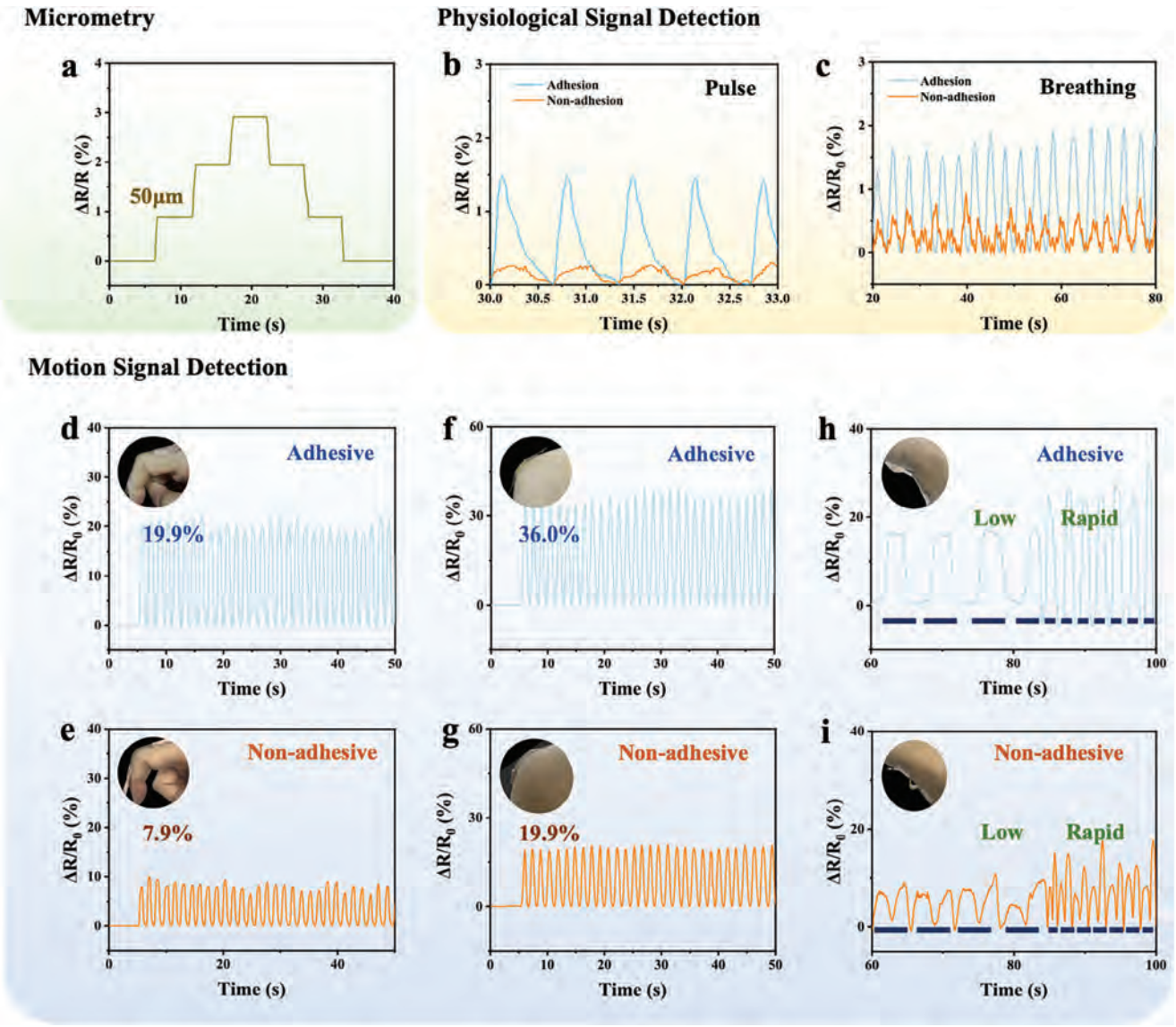

Figure 6. Micrometry: a) Relative resistance change of HP-Fe_0-Li_0/HP-$Fe_{5.5}$-$Li_{2.1}$ gradient eutectogel strain sensors at 50 μm stretching lengths. Physiological signal detection: b,c) Output of the self-adhering and nonadhering HP-Fe_0-Li_0/HP-$Fe_{5.5}$-$Li_{2.1}$ gradient eutectogel strain sensor for pulse and breathing. Motion signal detection: d–g) Output of the self-adhering and non-adhering HP-Fe_0-Li_0/HP-$Fe_{5.5}$-$Li_{2.1}$ gradient eutectogel strain sensor for monitoring the human finger and elbow. h,i) Output of the self-adhering and nonadhering HP-Fe_0-Li_0/HP-$Fe_{5.5}$-$Li_{2.1}$ gradient eutectogel strain sensors for the monitoring of fast and slow movements under the wrist.

stable signals (Figure 6h). In contrast, obvious detachment between the sensor and human skin was observed during bending, which led to the output signal disorders, especially when bending violently (Figure 6i).

2.7. Biocompatibility of the Gradient Eutectogel

HP-Fe_0-Li_0/HP-$Fe_{5.5}$-$Li_{2.1}$ gradient eutectogel strain sensors are in direct contact with the surface of the human skin during use. To confirm whether the eutectogel will have any effect on the human surface when it is used, we have carried out tests related to biocompatibility. According to **Figure** 7a, the eutectogel was fixed on the human body surface for 7 d, and there was only indentation on the human body surface without any allergic reactions. We performed a cytotoxicity test using the CCK8 method (Figure 7b). After 24 h, the relative cell viability of the experimental group was 84% of the control group. These results indicate that HP-Fe_0-Li_0/HP-$Fe_{5.5}$-$Li_{2.1}$ gradient eutectogel has excellent biocompatibility and can be used for long-term monitoring of human skin surface without any effect on human skin.

3. Conclusion

We developed a dual ion (Fe^{3+} and Li^+) regulation strategy to enhance the mechanical property of eutectogels, through which

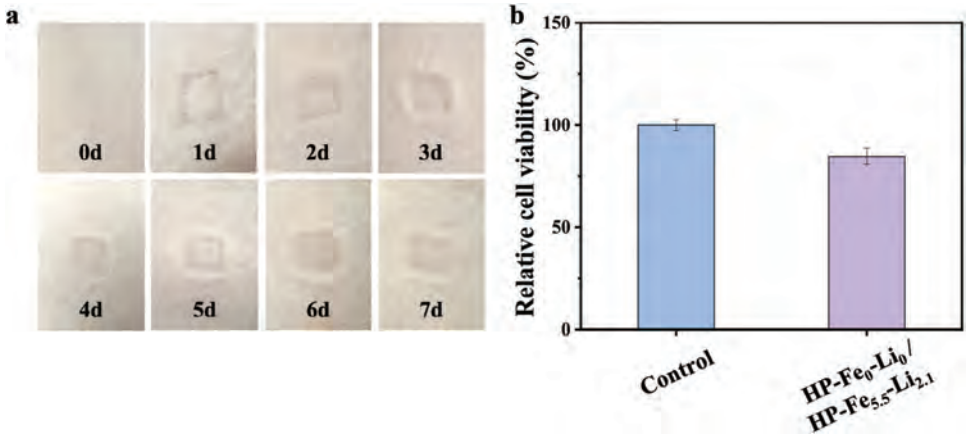

Figure 7. Biocompatibility of HP-Fe_0-Li_0/HP-$Fe_{5.5}$-$Li_{2.1}$ gradient eutectogel. a) Photographs of HP-Fe_0-Li_0/HP-$Fe_{5.5}$-$Li_{2.1}$ gradient eutectogel adhered to the surface of the skin for seven consecutive days. b) Cell viability for HP-Fe_0-Li_0/HP-$Fe_{5.5}$-$Li_{2.1}$ gradient eutectogel after 24 h of culture.

eutectogels with high elasticity (residual strain < 6%) and high adhesion (105 kPa on pigskin) were obtained. Strain sensors based on gradient eutectogels demonstrate high sensitivity (GF = 2.5), wide linear response range (150%), negligible electrical hysteresis, broad operational temperature range (−20–60 °C) and excellent environmental stability. Highly consistent signals were obtained at fixed strain regardless of loading or unloading, proving their potential in accurate micrometry. The self-adhesive property enabled the sensor to adapt to the complex conditions on human skin, facilitating its use as a wearable strain sensor for long-term monitoring of human activities.

Supporting Information

Supporting Information is available from the Wiley Online Library or from the author.

Acknowledgements

This work was financially supported by National Natural Science Foundation of China (Grant No 62122080 62261136551), Natural Science Foundation of Shanghai (22ZR1481700, 22dz1205000).

Conflict of Interest

The authors declare no conflict of interest.

Data Availability Statement

The data that support the findings of this study are available from the corresponding author upon reasonable request.

Keywords

eutectogels, high adhesion, low hysteresis, low residual strain, strain sensor

Received: January 30, 2024
Revised: April 29, 2024
Published online: May 22, 2024

[1] W. Wang, Y. Jiang, D. Zhong, Z. Zhang, S. Choudhury, J. C. Lai, H. Gong, S. Niu, X. Yan, Y. Zheng, C. C. Shih, R. Ning, Q. Lin, D. Li, Y. H. Kim, J. Kim, Y. X. Wang, C. Zhao, C. Xu, X. Ji, Y. Nishio, H. Lyu, J. B. Tok, Z. Bao, *Stem Cells Int.* **2023**, *380*, 735.
[2] X. Yu, Z. Xie, Y. Yu, J. Lee, A. Vazquez-Guardado, H. Luan, J. Ruban, X. Ning, A. Akhtar, D. Li, B. Ji, Y. Liu, R. Sun, J. Cao, Q. Huo, Y. Zhong, C. Lee, S. Kim, P. Gutruf, C. Zhang, Y. Xue, Q. Guo, A. Chempakasseril, P. Tian, W. Lu, J. Jeong, Y. Yu, J. Cornman, C. Tan, B. Kim, et al., *Nature* **2019**, *575*, 473.
[3] W. Zhang, B. Wu, S. Sun, P. Wu, *Nat. Commun.* **2021**, *12*, 4082.
[4] W. Asghar, F. Li, Y. Zhou, Y. Wu, Z. Yu, S. Li, D. Tang, X. Han, J. Shang, Y. Liu, R. W. Li, *Adv. Mater. Technol.* **2020**, *5*, 1900934.
[5] W. Zhai, C. Wang, S. Wang, J. Li, Y. Zhao, P. Zhan, K. Dai, G. Zheng, C. Liu, C. Shen, *J. Mater. Chem. A* **2021**, *9*, 7238.
[6] Y. Cai, J. Shen, G. Ge, Y. Zhang, W. Jin, W. Huang, J. Shao, J. Yang, X. Dong, *ACS Nano* **2018**, *12*, 56.
[7] L. Li, Y. Bai, L. Li, S. Wang, T. Zhang, *Adv. Mater.* **2017**, *29*, 1702517.
[8] R. Wang, N. Jiang, J. Su, Q. Yin, Y. Zhang, Z. Liu, H. Lin, F. A. Moura, N. Yuan, S. Roth, R. S. Rome, R. Ovalle-Robles, K. Inoue, S. Yin, S. Fang, W. Wang, J. Ding, L. Shi, R. H. Baughman, Z. Liu, *Adv. Funct. Mater.* **2017**, *27*, 1702134.
[9] Y. He, D. Wu, M. Zhou, Y. Zheng, T. Wang, C. Lu, L. Zhang, H. Liu, C. Liu, *ACS Appl. Mater. Interfaces* **2021**, *13*, 15572.
[10] C. Shao, M. Wang, L. Meng, H. Chang, B. Wang, F. Xu, J. Yang, P. Wan, *Chem. Mater.* **2018**, *30*, 3110.
[11] G. Tian, D. Yang, C. Liang, Y. Liu, J. Chen, Q. Zhao, S. Tang, J. Huang, P. Xu, Z. Liu, D. Qi, *Adv. Mater.* **2023**, *35*, 2212302.
[12] G. Cai, J. Wang, K. Qian, J. Chen, S. Li, P. S. Lee, *Adv. Sci.* **2017**, *4*, 1600190.
[13] Y. Zhang, Y. Wang, Y. Guan, Y. Zhang, *Nat. Commun.* **2022**, *13*, 6671.
[14] J. Song, S. Chen, L. Sun, Y. Guo, L. Zhang, S. Wang, H. Xuan, Q. Guan, Z. You, *Adv. Mater.* **2020**, *32*, 1906994.
[15] J. Wen, J. Tang, H. Ning, N. Hu, Y. Zhu, Y. Gong, C. Xu, Q. Zhao, X. Jiang, X. Hu, L. Lei, D. Wu, T. Huang, *Adv. Funct. Mater.* **2021**, *31*, 2011176.
[16] M. Liao, P. Wan, J. Wen, M. Gong, X. Wu, Y. Wang, R. Shi, L. Zhang, *Adv. Funct. Mater.* **2017**, *27*, 1703852.
[17] G. Ge, Y. Lu, X. Qu, W. Zhao, Y. Ren, W. Wang, Q. Wang, W. Huang, X. Dong, *ACS Nano* **2020**, *14*, 218.
[18] Y. Ye, Y. Zhang, Y. Chen, X. Han, F. Jiang, *Adv. Funct. Mater.* **2020**, *30*, 2003430.

[19] L. Han, K. Liu, M. Wang, K. Wang, L. Fang, H. Chen, J. Zhou, X. Lu, *Adv. Funct. Mater.* **2017**, *28*, 1704195.
[20] C. Huang, Q. Luo, Q. Miao, Z. He, P. Fan, Y. Chen, Q. Zhang, X. He, L. Li, X. Liu, *Polymer* **2022**, *253*, 124993.
[21] X. P. Morelle, W. R. Illeperuma, K. Tian, R. Bai, Z. Suo, J. J. Vlassak, *Adv. Mater.* **2018**, *30*, 1801541.
[22] L. Yang, L. Song, Y. Feng, M. Cao, P. Zhang, X.-F. Zhang, J. Yao, *J. Mater. Chem. A* **2020**, *8*, 12314.
[23] S. Xia, S. Song, Y. Li, G. Gao, *J. Mater. Chem. C* **2019**, *7*, 11303.
[24] Z. Zhang, Z. Gao, Y. Wang, L. Guo, C. Yin, X. Zhang, J. Hao, G. Zhang, L. Chen, *Macromolecules* **2019**, *52*, 2531.
[25] Z. Tian, L. Hou, D. Feng, Y. Jiao, P. Wu, *ACS Nano* **2023**, *17*, 3786.
[26] X. Chen, Y. K. Bai, C. Z. Zhao, X. Shen, Q. Zhang, *Angew. Chem.* **2020**, *132*, 11288.
[27] J. Mao, H. Tan, B. Yang, W. Zhang, X. Yang, Y. Zhang, H. Zhang, *Polymers* **2018**, *10*, 849.
[28] G. Chen, J. Huang, J. Gu, S. Peng, X. Xiang, K. Chen, X. Yang, L. Guan, X. Jiang, L. Hou, *J. Mater. Chem. A* **2020**, *8*, 6776.
[29] Y. Zhang, J. Mao, W. Jiang, S. Zhang, L. Tong, J. Mao, G. Wei, M. Zuo, Y. Ni, *Composites, Part B* **2021**, *217*, 108879.
[30] S. Liu, O. Oderinde, I. Hussain, F. Yao, G. Fu, *Polymer* **2018**, *144*, 111.
[31] J. Liu, S. Bao, Q. Ling, X. Fan, H. Gu, *Polymer* **2022**, *240*, 124513.
[32] S. Das, P. Martin, G. Vasilyev, R. Nandi, N. Amdursky, E. Zussman, *Macromolecules* **2020**, *53*, 11130.
[33] Y. Miao, M. Xu, L. Zhang, *Adv. Mater.* **2021**, *33*, 2102308.
[34] S. Xu, D. M. Vogt, W. H. Hsu, J. Osborne, T. Walsh, J. R. Foster, S. K. Sullivan, V. C. Smith, A. Rousing, E. C. Goldfield, R. J. Wood, *Adv. Funct. Mater.* **2019**, *29*, 1807058.
[35] G. Ge, Y. Zhang, J. Shao, W. Wang, W. Si, W. Huang, X. Dong, *Adv. Funct. Mater.* **2018**, *28*, 1802576.
[36] Y. Li, D. Wang, J. Wen, J. Liu, D. Zhang, J. Li, H. Chu, *Adv. Funct. Mater.* **2021**, *31*, 2011259.
[37] J. Huang, R. Zhou, Z. Chen, Y. Wang, Z. Li, X. Mo, N. Gao, J. He, C. Pan, *Mater. Today Phys.* **2023**, *35*, 101123.
[38] J. Lee, S. J. Ihle, G. S. Pellegrino, H. Kim, J. Yea, C.-Y. Jeon, H.-C. Son, C. Jin, D. Eberli, F. Schmid, B. L. Zambrano, A. F. Renz, C. Forró, H. Choi, K.-I. Jang, R. Küng, J. Vörös, *Nat. Electron.* **2021**, *4*, 291.
[39] J. Gao, Y. Fan, Q. Zhang, L. Luo, X. Hu, Y. Li, J. Song, H. Jiang, X. Gao, L. Zheng, W. Zhao, Z. Wang, W. Ai, Y. Wei, Q. Lu, M. Xu, Y. Wang, W. Song, X. Wang, W. Huang, *Adv-. Mater.* **2022**, *34*, 2107511.
[40] H. He, T. Yang, T. Liu, Y. Gao, Z. Zhang, Z. Yang, F. Liang, *Adv. Mater.* **2024**, *36*, 2312278.
[41] D. Kim, J. Yoon, *ACS Appl. Mater. Interfaces* **2020**, *12*, 20965.
[42] X. Shi, H. Wang, X. Xie, Q. Xue, J. Zhang, S. Kang, C. Wang, J. Liang, Y. Chen, *ACS Nano* **2019**, *13*, 649.